Available online at www.sciencedirect.com
SCIENCE DIRECT®
Journal of Computational Physics 207 (2005) 69–91
JOURNAL OF COMPUTATIONAL PHYSICS
www.elsevier.com/locate/jcp

TE/TM scheme for computation of electromagnetic fields in accelerators

Igor Zagorodnov *,[1], Thomas Weiland

Technische Universitaet Darmstadt, Fachbereich Elektrotechnik und Informationstechnik, Institut fuer Theorie Elektromagnetischer Felder (TEMF), Schlossgartenstrasse 8, D-64289 Darmstadt, Germany

Received 28 June 2004; received in revised form 12 January 2005; accepted 12 January 2005
Available online 16 February 2005

Abstract

We propose a new two-level economical conservative scheme for short-range wake field calculation in three dimensions. The scheme does not have dispersion in the longitudinal direction and is staircase free (second order convergent). Unlike the finite-difference time domain method (FDTD), it is based on a TE/TM like splitting of the field components in time. Additionally, it uses an enhanced alternating direction splitting of the transverse space operator that makes the scheme computationally as effective as the conventional FDTD method. Unlike the FDTD ADI and low-order Strang methods, the splitting error in our scheme is only of fourth order. As numerical examples show, the new scheme is much more accurate on the long-time scale than the conventional FDTD approach.

Keywords: Maxwell's equations; FDTD; ADI; Finite integration; Conformal; Wake field

1. Introduction

External electromagnetic (EM) fields are used to store and accelerate beams of charged particles. However, the particles themselves are field sources. When traversed by charged particles, cross-section variations of the vacuum chamber wall generate EM fields which are called wake fields since they remain usually behind the exciting particles. These wake fields influence the motion of trailing particles that may lead to beam instabilities [1]. Without good knowledge of these wake fields and of their interactions, an accelerator can hardly be operated at the desired top performance. The only practical way of calculating and studying the EM fields in real structures is the application of numerical methods. The first numerical codes were

* Corresponding author. Tel.: +49 6151 164 787; fax: +49 6151 164 611.
E-mail addresses: zagor@temf.de (I. Zagorodnov), thomas.weiland@temf.de (T. Weiland).
[1] Work supported in part by the Deutsche Forschungsgemeinschaft, project WE1239/22-1.

0021-9991/$ - see front matter © 2005 Published by Elsevier Inc.
doi:10.1016/j.jcp.2005.01.003

developed at the end of the seventies [2,3]; later on a lot of sophisticated computer codes based on several numerical techniques have been elaborated.

However, the computation of wakes of short relativistic bunches in long structures remains a challenging problem even with the fastest computers available. It demands developing new numerical approaches for long-time calculation of electromagnetic fields in the vicinity of relativistic bunches. The conventional FDTD scheme [4], used in MAFIA [5], TBCI [6] and other wake and particle-in-cell (PIC) codes, suffers from numerical grid dispersion and the staircase approximation problem.

Several approaches [7–10] have been proposed to reduce the accumulated dispersion error of large-scale three-dimensional simulations for *all* angles and for a *given* frequency range. These methods require the usage of larger spatial stencils and a special treatment of the material interfaces. The increased computational burden justifies itself for computational domains large in all three dimensions. However, in the accelerator applications the domain of interest is very long in the longitudinal direction and relatively short in the transverse plane. Additionally, the electromagnetic field changes very fast in the direction of bunch motion but is relatively smooth in the transverse plane. Hence, it is extremely important to eliminate the dispersion error in the longitudinal direction for *all* frequencies. As well known, the FDTD method at the Courant limit is dispersion free along grid diagonals and this property can be used effectively in numerical simulations [11]. However, the only reasonable choice in this case is to take equal mesh steps in all three directions.

Alternatively, a semi-implicit numerical scheme without dispersion in the longitudinal direction with a simpler conformal treatment of material interfaces and the usage of non-equidistant grids has been developed in [12–15].

The scheme described in [13] allows to solve the scalar problem and calculate the wake potential for fully axially symmetric problems with staircase approximation of the boundary. In [14,15], a three-level conformal (second order convergent) scheme

$$\mathbf{R}(\mathbf{y}^{n+1} - 2\mathbf{y}^n + \mathbf{y}^{n-1}) + \mathbf{A}\mathbf{y}^n = \mathbf{f}^n$$

for the vectorial problem was suggested. The scheme is based on a vector potential formulation and allows an economical realization for axially symmetric geometries. However, the operator $\mathbf{R}$ in the scheme is not self-conjugate; and therefore an "energy" conservation cannot be proved theoretically by the standard techniques [16]. Additionally, the scheme is not economical for general three-dimensional geometries. The last drawback can be overcome by splitting methods [17]. However, the absence of a theoretical proof for an energy conservation has stimulated us to look for an alternative approach in the three-dimensional case.

In this paper, a new two-level economical conservative scheme for short-range wake field calculations in three dimensions is presented. The scheme does not have dispersion in the longitudinal direction and is staircase free (second order convergent). Unlike the FDTD method [4] and the scheme developed in [14,15], the new method is based on a TE/TM ("transversal electric–transversal magnetic") like splitting of the field components in time. Additionally, it uses an enhanced alternating direction splitting of the transverse space operator that renders the scheme computationally as effective as the conventional FDTD method. Unlike the FDTD ADI [18] and low-order Strang [19] methods, the splitting error in our scheme is only of fourth order. Numerical examples show that the new scheme is much more accurate in long-time simulations than the conventional FDTD approach. For axially symmetric geometries, the new scheme performs at least two times faster than the scheme suggested in [14,15] while achieving the same level of accuracy.

2. Formulation of the problem

At high energies the particle beam is rigid. To obtain the wake field, the Maxwell equations can be solved with a rigid particle distribution. The influence of the wake field on the particle distribution is neglected

here; thus, the beam-surroundings system is not solved self-consistently and a mixed Cauchy problem for the situation shown in Fig. 1 should be considered.

The problem reads: for a bunch moving with the velocity of light c and characterized by a charge distribution ρ find the electromagnetic field $\vec{E},\vec{H}$ in a domain Ω which is bounded transversally by a perfect conductor $\partial\Omega$. The bunch introduces an electric current $\vec{j}=\vec{c}\rho$ and thus we have to solve for

$$\begin{aligned}
&\nabla\times\vec{H}=\frac{\partial}{\partial t}\vec{D}+\vec{j},\quad \nabla\times\vec{E}=-\frac{\partial}{\partial t}\vec{B},\\
&\nabla\cdot\vec{D}=\rho,\quad \nabla\cdot\vec{B}=0,\\
&\vec{H}=\mu^{-1}\vec{B},\quad \vec{D}=\varepsilon\vec{E},\quad x\in\Omega,\\
&\vec{E}(t=0)=\vec{E}_0,\quad \vec{H}(t=0)=\vec{H}_0,\quad x\in\bar{\Omega},\\
&\vec{n}\times\vec{E}=0,\quad x\in\partial\Omega,
\end{aligned}\tag{1}$$

where $\vec{E}_0,\ \vec{H}_0$ is an initial electromagnetic field in domain $\overline{\Omega}$.

The shape of the field distribution of a relativistic point charge q in free space resembles a pancake moving with the charge. For the charge moving along the z-axis only two field components are presented in cylindrical coordinates (z,r,θ) [20]

$$\vec{E}_r^{0,q}(\vec{r},t)=c\vec{B}_\theta^{0,q}(\vec{r},t)=\frac{Z_0 q}{2\pi r}\delta(z-ct).$$

Hence, the free space field for the linear charge distribution $\rho\ (z,r,\theta,t)=\delta(r)\rho_z(z-ct)$ reads:

$$\vec{E}_r^0(\vec{r},t)=\frac{Z_0}{2\pi r}\rho_z(z-ct),\ c\vec{B}_\theta^0(\vec{r},t)=\vec{E}_r^0(\vec{r},t).$$

For a bunch $\rho(z,r,\theta,t)=\delta(a)\delta(\theta)\rho_z(z-ct)$ moving at an offset a from the z-axis the free space field can be written in the form

$$\begin{aligned}
&\vec{E}_r^0(\vec{r},t)=\frac{Z_0}{2\pi}\frac{\rho_z(z-ct)(r-a\cos\theta)}{a^2+r^2-2ar\cos\theta},\quad \vec{E}_\theta^0(\vec{r},t)=\frac{Z_0}{2\pi}\frac{\rho_z(z-ct)a\sin\theta}{a^2+r^2-2ar\cos\theta},\\
&cB_r^0(\vec{r},t)=-\vec{E}_\theta^0(\vec{r},t),\quad cB_\theta^0(\vec{r},t)=\vec{E}_r^0(\vec{r},t).
\end{aligned}\tag{2}$$

In accelerator applications, the studied structure is usually supplied by ingoing pipe and the analytical solution in a perfectly conducting cylindrical pipe [20] can be used as initial condition

$$\begin{aligned}
&\vec{E}_{0,r}(\vec{r},0)=\vec{E}_r^0(\vec{r},0)+\frac{Z_0}{2\pi}\frac{\rho_z(z)a(-ar+b^2\cos\theta)}{b^4+a^2r^2-2arb^2\cos\theta},\\
&\vec{E}_{0,\theta}(\vec{r},0)=\vec{E}_\theta^0(\vec{r},0)-\frac{Z_0}{2\pi}\frac{\rho_z(z)ab^2\sin\theta}{b^4+a^2r^2-2arb^2\cos\theta},\\
&cB_{0,\theta}(\vec{r},0)=\vec{E}_{0,r}(\vec{r},0),\quad cB_{0,r}(\vec{r},0)=-\vec{E}_{0,\theta}(\vec{r},0).
\end{aligned}\tag{3}$$

If the ingoing pipe is not cylindrical the initial field can be found numerically.

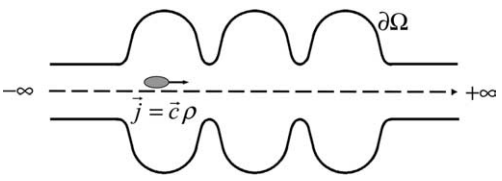

Fig. 1. Charged particle bunch moving through an accelerating structure supplied with infinite pipes.

3. Implicit TE/TM numerical scheme

3.1. Finite integration technique

Following the matrix notation of the finite integration technique (FIT) [21], the Cauchy problem (1) can be approximated by the *time-continuous* matrix equations on a grid doublet $(G, \widetilde{G})$

$$\begin{aligned} &\mathbf{C}\,\widehat{e} = -\frac{\mathrm{d}}{\mathrm{d}t}\widehat{\mathbf{b}}, \quad \mathbf{C}^*\,\widehat{\mathbf{h}} = \frac{\mathrm{d}}{\mathrm{d}t}\widehat{\mathbf{d}} + \widehat{\mathbf{j}}, \\ &S\,\widehat{\mathbf{b}} = \mathbf{0}, \; \mathbf{S}^*\,\widehat{\mathbf{d}} = \mathbf{q}. \end{aligned} \tag{4}$$

completed by the discrete form of the material relations (constitutive equations)

$$\widehat{\mathbf{e}} = \mathbf{M}_{\varepsilon^{-1}}\,\widehat{\mathbf{d}}, \quad \widehat{\mathbf{h}} = \mathbf{M}_{\mu^{-1}}\,\widehat{\mathbf{b}}$$

with the discrete inverse permittivity matrix $\mathbf{M}_{\varepsilon^{-1}}$ and the inverse permeability matrix $\mathbf{M}_{\mu^{-1}}$. In the following the material matrices are assumed to be real and symmetric.

On Cartesian $\{x, y, z\}$-coordinate grids (like the Cartesian grid shown in Fig. 2) with an appropriate indexing scheme the curl matrix has an 3×3 block structure:

$$\mathbf{C} = \begin{pmatrix} \mathbf{0} & -\mathbf{P}_z & \mathbf{P}_y \\ \mathbf{P}_z & \mathbf{0} & -\mathbf{P}_x \\ -\mathbf{P}_y & \mathbf{P}_x & \mathbf{0} \end{pmatrix}.$$

The two-banded topological $\mathbf{P}_{\{x,y,z\}}$-matrices play the role of discrete partial differential-operators [22].

With changing of variables $\mathbf{e} = \mathbf{M}_{\varepsilon^{-1}}^{-1/2}\,\widehat{\mathbf{e}}$, $\mathbf{h} = \mathbf{M}_{\mu^{-1}}^{-1/2}\,\widehat{\mathbf{h}}$, $\mathbf{j} = c^{-1}\mathbf{M}_{\varepsilon^{-1}}^{1/2}\,\widehat{\mathbf{j}}$, $\tau = ct$, system (4) reduces to the skew-symmetric one

$$\frac{\mathrm{d}}{\mathrm{d}\tau}\mathbf{e} = \mathbf{C}_0^*\mathbf{h} + \mathbf{j}, \quad \frac{\mathrm{d}}{\mathrm{d}\tau}\mathbf{h} = -\mathbf{C}_0\mathbf{e} \tag{5}$$

with a new "discrete curl" matrix

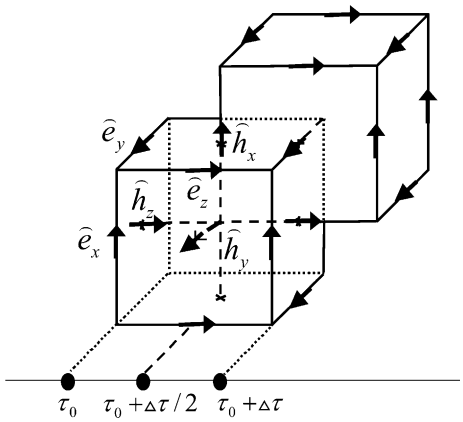

Fig. 2. Positions of the relativistic charged particle in the FIT grid in different moments of time. The scaled time step is chosen equal to the longitudinal mesh step.

$$\mathbf{C}_0 = c^{-1}\mathbf{M}_{\mu^{-1}}^{1/2}\mathbf{C}\mathbf{M}_{\varepsilon^{-1}}^{1/2} = c^{-1}\begin{pmatrix} \mathbf{0} & -\mathbf{M}_{\mu_x^{-1}}^{1/2}\mathbf{P}_z\mathbf{M}_{\varepsilon_y^{-1}}^{1/2} & \mathbf{M}_{\mu_x^{-1}}^{1/2}\mathbf{P}_y\mathbf{M}_{\varepsilon_z^{-1}}^{1/2} \\ \mathbf{M}_{\mu_y^{-1}}^{1/2}\mathbf{P}_z\mathbf{M}_{\varepsilon_x^{-1}}^{1/2} & \mathbf{0} & -\mathbf{M}_{\mu_y^{-1}}^{1/2}\mathbf{P}_x\mathbf{M}_{\varepsilon_z^{-1}}^{1/2} \\ -\mathbf{M}_{\mu_z^{-1}}^{1/2}\mathbf{P}_y\mathbf{M}_{\varepsilon_x^{-1}}^{1/2} & \mathbf{M}_{\mu_z^{-1}}^{1/2}\mathbf{P}_x\mathbf{M}_{\varepsilon_y^{-1}}^{1/2} & \mathbf{0} \end{pmatrix} \equiv \begin{pmatrix} \mathbf{0} & -\mathbf{P}_z^0 & \mathbf{P}_y^0 \\ \mathbf{P}_z^1 & \mathbf{0} & -\mathbf{P}_x^0 \\ -\mathbf{P}_y^1 & \mathbf{P}_x^1 & \mathbf{0} \end{pmatrix}.$$

System (5) is a *time-continuous* and *space-discrete* approximation of problem (1). The next step is a discretization of the system in time. The field components can be split in time and the "leap-frog" scheme can be applied. Below, two kinds of the splitting are considered: E/M and TE/TM schemes.

3.2. Explicit FDTD method based on "electric–magnetic" splitting of the field components in time

Suggested by Yee [4], the E/M ("electric–magnetic") splitting of the field components yields the *explicit* FDTD scheme (E/M scheme)

$$\mathbf{e}^{n+0.5} = \mathbf{e}^{n-0.5} + \Delta\tau\mathbf{C}_0^*\mathbf{h}^n + \Delta\tau\mathbf{j}^n, \quad \mathbf{h}^{n+1} = \mathbf{h}^n - \Delta\tau\mathbf{C}_0\mathbf{e}^{n+0.5} \tag{6}$$

where $\Delta\tau$ is the time step and the update of the electric components is shifted by $0.5\Delta\tau$ relative to update of the magnetic components.

Scheme (6) is a two-layer scheme

$$\mathbf{B}\frac{\mathbf{y}^{n+1}-\mathbf{y}^n}{\Delta\tau} + \mathbf{A}\mathbf{y}^n = \mathbf{f}^n, \tag{7}$$

where

$$\mathbf{B} = \begin{pmatrix} \mathbf{I} & \mathbf{0} \\ \Delta\tau\mathbf{C}_0 & \mathbf{I} \end{pmatrix}, \mathbf{A} = \begin{pmatrix} \mathbf{0} & -\mathbf{C}_0^* \\ \mathbf{C}_0 & \mathbf{0} \end{pmatrix}, \mathbf{y}^n = \begin{pmatrix} \mathbf{e}^{n-0.5} \\ \mathbf{h}^n \end{pmatrix}, \mathbf{f}^n = \begin{pmatrix} \mathbf{j}^n \\ \mathbf{0} \end{pmatrix}.$$

We study the stability of scheme (7) by the energy inequalities method [16]. Let us take the inner product of both sides in Eq. (7) with $\mathbf{y}^{n+1} + \mathbf{y}^n$:

$$\langle \mathbf{B}(\mathbf{y}^{n+1}-\mathbf{y}^n), \mathbf{y}^{n+1}+\mathbf{y}^n\rangle + \Delta\tau\langle \mathbf{A}\mathbf{y}^n, \mathbf{y}^{n+1}+\mathbf{y}^n\rangle = \langle \Delta\tau\mathbf{f}^n, \mathbf{y}^{n+1}+\mathbf{y}^n\rangle. \tag{8}$$

Using the formula

$$\mathbf{y}^n = 0.5((\mathbf{y}^{n+1}+\mathbf{y}^n) - (\mathbf{y}^{n+1}-\mathbf{y}^n))$$

we rewrite relation (8) in the form

$$\langle [\mathbf{B} - 0.5\Delta\tau\mathbf{A}](\mathbf{y}^{n+1}-\mathbf{y}^n), \mathbf{y}^{n+1}+\mathbf{y}^n\rangle + 0.5\Delta\tau\langle \mathbf{A}(\mathbf{y}^{n+1}+\mathbf{y}^n), \mathbf{y}^{n+1}+\mathbf{y}^n\rangle = \langle \Delta\tau\mathbf{f}^n, \mathbf{y}^{n+1}+\mathbf{y}^n\rangle.$$

The second term in the left-hand side is equal to zero since the operator $\mathbf{A}$ is skew-symmetric and, therefore,

$$\langle \mathbf{Q}\mathbf{y}^{n+1}, \mathbf{y}^{n+1}\rangle - \langle \mathbf{Q}\mathbf{y}^n, \mathbf{y}^n\rangle = \langle \Delta\tau\mathbf{f}^n, \mathbf{y}^{n+1}+\mathbf{y}^n\rangle,$$

where the self-adjointness of the operator $\mathbf{Q} \equiv B - 0.5\Delta\tau\mathbf{A}$ is used.

The last relation allows to prove

Theorem 1. *The condition*

$$\mathbf{Q} \equiv \mathbf{B} - 0.5\Delta\tau\mathbf{A} \geqslant 0 \tag{9a}$$

is necessary and sufficient for the stability in the Hilbert space H_Q (see [16]) of scheme (8) with respect to the initial data $\mathbf{y}^0$ and the right-hand side $\mathbf{f}^n$. For a solution of problem (8) the a priori estimate holds

$$\|\mathbf{y}^{n+1}\|_{\mathbf{Q}} \leqslant \|\mathbf{y}^{n}\|_{\mathbf{Q}} + \sum_{k=0}^{n} C\|\mathbf{f}^{k}\|_{\mathbf{Q}}. \tag{9b}$$

Following [23,24], a discrete energy of electromagnetic fields can be defined as

$$\mathrm{E}^{n}_{\mathrm{E/M}} = 0.5\langle[\mathbf{B} - 0.5\Delta\tau\mathbf{A}]\mathbf{y}^{n}, \mathbf{y}^{n}\rangle = 0.5(\langle\mathbf{e}^{n-0.5}, \mathbf{e}^{n-0.5}\rangle + \langle\mathbf{h}^{n}, \mathbf{h}^{n-1}\rangle). \tag{10}$$

Note that this energy has a close correspondence to the total physical energy of the continuous electromagnetic fields given by $0.5\int_V(\varepsilon|E|^2 + \mu^{-1}|B|^2)\,\mathrm{d}v$. If the right-hand side in scheme (7) is zero then the scheme is energy conserving

$$E^{n}_{\mathrm{E/M}} = E^{0}_{\mathrm{E/M}}.$$

The condition (9a) can be rewritten as

$$\frac{\tau^2}{4}\mathbf{C}_0\mathbf{C}_0^{*}\mathbf{I} \text{ or } \Delta\tau\frac{2}{\sqrt{\max\lambda_i}},$$

where $\{\lambda_i\}$ are eigenvalues of the matrix $\mathbf{C}_0\mathbf{C}_0^{*}$.

The last inequalities are direct corollaries of

Lemma 1. *Let us define a matrix* $\widetilde{\mathbf{A}}$ *by relation*

$$\widetilde{\mathbf{A}} = \begin{pmatrix} \mathbf{0} & \mathbf{A} \\ \mathbf{A}^{*} & \mathbf{0} \end{pmatrix}$$

For the square matrix $\mathbf{A}$ *the conditions*

(a) $\mathbf{I} + \widetilde{\mathbf{A}} \geqslant \mathbf{0}$ *and*
(b) $\mathbf{I} - \mathbf{A}^{*}\mathbf{A} \geqslant \mathbf{0}$

are equivalent.

Indeed, the set $\{\widetilde{\lambda_i^{A}}\}$ of eigenvalues of the matrix $\widetilde{\mathbf{A}}$ can be written in the form

$$\{\widetilde{\lambda_i^{\mathbf{A}}}\} = \left\{\sqrt{\lambda_i^{\mathbf{A}^{*}\mathbf{A}}}\right\} \oplus \left\{-\sqrt{\lambda_i^{\mathbf{A}^{*}\mathbf{A}}}\right\},$$

where $\{\lambda_i^{\mathbf{A}^{*}\mathbf{A}}\}$ is a set of eigenvalues of the non-negative self-conjugate matrix $\mathbf{A}^{*}\mathbf{A}$. Hence, both relations (a) and (b) hold simultaneously.

It was proven in [24] that relation (9a), (9b) holds if

$$\Delta\tau \leqslant c^{-1}\min_{\xi}\sqrt{\frac{\mu_\xi\varepsilon_\xi}{\Delta x_\xi^{-2} + \Delta y_\xi^{-2} + \Delta z_\xi^{-2}}}, \xi = (i, j, k). \tag{11}$$

Scheme (6) is widely used in electromagnetic modeling. However, the FDTD algorithm causes non-physical dispersion of the simulated waves in a free-space computational lattice. The phase velocity of discrete wave modes can differ from the light velocity by an amount varying with the wavelength, direction of propagation in the grid and grid discretization. With an equidistant mesh, a homogenous material and the time step equal to the right-hand side of inequality (11), the scheme has zero dispersion along the grid diagonals. Hence, the zero dispersion in a desired direction can be achieved by rotation of the mesh. However, this approach awakes limitations on discretization: the only reasonable choice in this case is to take equal mesh steps in the all three directions. The next difficulty arises with the attempt to use a conformal method.

Why is zero dispersion for a special direction important? Unlike plasma problems, the charged particles in accelerators are organized and a direction of motion (the longitudinal direction) can be identified. Hence, the computational domain is very long in the longitudinal direction and relatively short in the transverse plane. Additionally, the electromagnetic field changes very fast in the direction of motion but is relatively smooth in the transverse plane.

Note also that to be able to model smooth transitions in geometry we should use a conformal approach without time step reduction [25].

3.3. Implicit FDTD method based on "transversal electric–transversal magnetic" splitting of the field components in time

The arguments, stated in the preceding section, force us to look for a numerical scheme, which

- does not have dispersion in the longitudinal direction;
- allows the use of non-homogeneous meshes in the transverse plane;
- allows the use of a moving mesh without interpolations;
- allows accurate geometry modeling without a time step reduction.

In [14,15], a three-level implicit conformal scheme

$$\mathbf{R}(\mathbf{y}^{n+1} - 2\mathbf{y}^n + \mathbf{y}^{n-1}) + \mathbf{A}\mathbf{y}^n = \mathbf{f}^n$$

was suggested. The scheme is based on a vector potential formulation and allows an economical realization for axially symmetric geometries. However, the absence of a theoretical proof for an energy conservation has stimulated us to look for an alternative approach in the three-dimensional case.

To find an alternative scheme, let us consider Fig. 2 and subdue an update procedure to the motion of the bunch. We suggest that a charged particle is moving in the z-direction with velocity of light. Additionally, let us suggest that our numerical scheme allows to take a time step $\Delta\tau$ equal to the mesh step z in the z-direction. If at the time τ_0 the particle has the position aligned with the left z-facet of the primary grid (see Fig. 2), then at time $\tau_0 + 0.5\Delta\tau$ it will be aligned with the left z-facet of the dual grid and in the time $\tau_0 + \Delta\tau$ it will be again aligned with the next z-facet of the primary grid. This suggests that we should replace the E/M time splitting of the field components in scheme (6) by a more adequate TE/TM splitting. Indeed, at time τ_0 it is reasonable to update the "TE" components $\mathbf{e}_x$, $\mathbf{e}_y$, $\mathbf{h}_z$ and half a time step later, namely at time $\tau_0 + 0.5\Delta\tau$, we have to update the "TM" components h_x, $\mathbf{h}_y$, $\mathbf{e}_z$.

Following these consideration, let us rewrite scheme (5) in the equivalent form

$$\frac{\mathrm{d}}{\mathrm{d}\tau}\mathbf{u} = \mathbf{D}_{11}\mathbf{u} + \mathbf{D}_{12}\mathbf{v} + \mathbf{j}_u, \quad \frac{\mathrm{d}}{\mathrm{d}\tau}\mathbf{v} = \mathbf{D}_{22}\mathbf{v} + \mathbf{D}_{21}\mathbf{u} + \mathbf{j}_v \tag{12}$$

where

$$\mathbf{D}_{11} = \begin{pmatrix} \mathbf{0} & \mathbf{0} & -\mathbf{P}_y^0 \\ \mathbf{0} & \mathbf{0} & \mathbf{P}_x^0 \\ \left(\mathbf{P}_y^0\right)^* & -\left(\mathbf{P}_x^0\right)^* & \mathbf{0} \end{pmatrix}, \quad \mathbf{D}_{22} = \begin{pmatrix} \mathbf{0} & \mathbf{0} & -(\mathbf{P}_y^1)^* \\ \mathbf{0} & \mathbf{0} & (\mathbf{P}_x^1)^* \\ \mathbf{P}_y^1 & -\mathbf{P}_x^1 & \mathbf{0} \end{pmatrix},$$

$$\mathbf{D}_{12} = -\mathbf{D}_{21}^* = \begin{pmatrix} \mathbf{0} & \mathbf{P}_z^0 & \mathbf{0} \\ -\mathbf{P}_z^1 & \mathbf{0} & \mathbf{0} \\ \mathbf{0} & \mathbf{0} & \mathbf{0} \end{pmatrix}, \quad \mathbf{u} = \begin{pmatrix} \mathbf{h}_x \\ \mathbf{h}_y \\ \mathbf{e}_z \end{pmatrix}, \quad \mathbf{v} = \begin{pmatrix} \mathbf{e}_x \\ \mathbf{e}_y \\ \mathbf{h}_z \end{pmatrix}, \quad \mathbf{j}_u = \begin{pmatrix} \mathbf{0} \\ \mathbf{0} \\ -\mathbf{j}_z \end{pmatrix}, \quad \mathbf{j}_v = \begin{pmatrix} -\mathbf{j}_x \\ -\mathbf{j}_y \\ \mathbf{0} \end{pmatrix}.$$

Applying the suggested TE/TM splitting of the field in time to system (12), the following numerical scheme is obtained

$$\frac{\mathbf{u}^{n+0.5}-\mathbf{u}^{n-0.5}}{\tau}=\mathbf{D}_{11}\frac{\mathbf{u}^{n+0.5}+\mathbf{u}^{n-0.5}}{2}+\mathbf{D}_{12}\mathbf{v}^{n}+\mathbf{j}_{u}^{n}, \tag{13a}$$

$$\frac{\mathbf{v}^{n+1}-\mathbf{v}^{n}}{\tau}=\mathbf{D}_{22}\frac{\mathbf{v}^{n+1}+\mathbf{v}^{n}}{2}+\mathbf{D}_{21}\mathbf{u}^{n+0.5}+\mathbf{j}_{v}^{n+0.5} \tag{13b}$$

Just like scheme (6), scheme (13a), (13b) is also a two-layer one

$$\mathbf{B}\frac{\mathbf{y}^{n+1}-\mathbf{y}^{n}}{\Delta\tau}+\mathbf{A}\mathbf{y}^{n}=\mathbf{f}^{n}, \tag{14}$$

where

$$\mathbf{B}=\begin{pmatrix}\mathbf{I}-0.5\tau\mathbf{D}_{11} & \mathbf{0}\\ \Delta\tau\mathbf{D}_{12}^{*} & \mathbf{I}-0.5\Delta\tau\mathbf{D}_{22}\end{pmatrix},\mathbf{A}=\begin{pmatrix}-\mathbf{D}_{11} & -\mathbf{D}_{12}\\ \mathbf{D}_{12}^{*} & -\mathbf{D}_{22}\end{pmatrix},\mathbf{y}^{n}=\begin{pmatrix}\mathbf{u}^{n-0.5}\\ \mathbf{v}^{n}\end{pmatrix},\mathbf{f}^{n}=\begin{pmatrix}\mathbf{j}_{u}^{n}\\ \mathbf{j}_{v}^{n+0.5}\end{pmatrix}.$$

Analyzing relations (14) we conclude that just as for the Yee's scheme the following relations hold

$$\mathbf{A}=-\mathbf{A}^{*},\mathbf{Q}=\mathbf{Q}^{*},\mathbf{Q}=\mathbf{B}-0.5\Delta\tau\mathbf{A}.$$

Likewise we can prove

Theorem 2. *The condition (9a) is necessary and sufficient for the stability in space H_Q of scheme (14) with respect to the initial data $\mathbf{y}^0$ and to the right-hand side $\mathbf{f}^n$. For a solution of problem (14) the a priori estimate (9b) holds.*

As for the E/M scheme the discrete energy in the TE/TM scheme can be defined by the relation

$$E_{\mathrm{TE/TM}}^{n}=0.5\langle[\mathbf{B}-0.5\Delta\tau\mathbf{A}]\mathbf{y}^{n},\mathbf{y}^{n}\rangle=E_{\mathrm{E/M}}^{n}+\mathrm{O}(\Delta\tau^{2}).$$

Note that the energy $E_{\mathrm{TE/TM}}^{n}$, just like the energy $E_{\mathrm{E/M}}^{n}$ defined by relation (10), is a second order accurate approximation to the total physical energy of the continuous electromagnetic field. If the right-hand side in scheme (14) vanishes, the scheme is energy conserving:

$$E_{\mathrm{TE/TM}}^{n}=E_{\mathrm{TE/TM}}^{0}.$$

Due to Lemma 1 stability condition (9a), (9b) can be rewritten in the form

$$\mathbf{I}-\frac{\Delta\tau^{2}}{4}\mathbf{D}_{12}\mathbf{D}_{12}^{*}\geqslant 0\quad\text{or}\quad\mathbf{I}-\frac{\Delta\tau^{2}}{4}\mathbf{P}_{z}^{i}\left(\mathbf{P}_{z}^{i^{*}}\right)\geqslant 0,\quad i=0,1. \tag{15}$$

The last relation resembles the well-known stability condition of the explicit FDTD scheme for the one-dimensional problem. In the following an equal mesh step Δz in the z-direction will always be assumed. Then for a vacuum domain with *staircase* approximation of the boundary the stability condition reads

$$\Delta\tau\leqslant\Delta z. \tag{16}$$

With the time step $\Delta\tau$ equal to the longitudinal mesh step Δz, scheme (13a), (13b) does not have dispersion in the longitudinal direction. Relation (15) does not contain information about the transverse mesh. Hence, the transverse mesh can be chosen independently from stability considerations.

For a relativistic bunch a mesh moving together with the bunch can be used. The field ahead of the bunch is zero and, as the scaled time step is equal to the longitudinal mesh step, the complete information for updating of the last mesh layer is available, too. It means that interpolation procedures are avoided and the dispersion in the longitudinal direction is equal to zero. The results with the moving mesh for staircase approximation of the geometry are fully equivalent to the stationary global mesh approach.

So far we have found a scheme which with staircase geometry approximation fulfills the first three requirements formulated above. However, in a general case the staircase scheme is only first order accurate. In order to overcome this problem and avoid reduction of the stable time step, the uniformly stable conformal (USC) approach described in [15,25] will be used.

With the latter approach the scheme possesses the desired features. However, it is implicit and non-economical. The economical scheme modifications, based on operator splitting, will be considered in the next sections.

4. An economical TE/TM scheme based on transverse operator splitting

4.1. Crank–Nicholson scheme for two-dimensional scalar wave equation as a basic part of the TE/TM scheme

In the following it is assumed that the transverse current $\mathbf{j}_v^{n+0.5} \equiv 0$ and only relation (13b) for "TE"-components is treated. It can be rewritten in the form

$$(\mathbf{I} - 0.5\Delta\tau\mathbf{D}_{22})\frac{\mathbf{v}^{n+1} - \mathbf{v}^n}{\Delta\tau} = \mathbf{D}_{22}\mathbf{v}^n - \mathbf{D}_{12}^*\mathbf{u}^{n+0.5}, \tag{17}$$

where

$$(\mathbf{I} - 0.5\Delta\tau\mathbf{D}_{22}) = \begin{pmatrix} \mathbf{I} & \mathbf{0} & 0.5\Delta\tau(\mathbf{P}_y^1)^* \\ \mathbf{0} & \mathbf{I} & -0.5\Delta\tau(\mathbf{P}_x^1)^* \\ -0.5\tau\mathbf{P}_y^1 & 0.5\Delta\tau\mathbf{P}_x^1 & \mathbf{I} \end{pmatrix} \tag{18}$$

Elimination of non-diagonal elements in the last row of matrix (18) in scheme (17) leads to

$$\frac{e_x^{n+1} - \mathbf{e}_x^n}{\Delta\tau} = \left(\mathbf{P}_z^1\right)^*\mathbf{h}_y^{n+0.5} - (\mathbf{P}_y^1)^*\frac{h_z^{n+1} + \mathbf{h}_z^n}{2}, \tag{19a}$$

$$\frac{e_y^{n+1} - \mathbf{e}_y^n}{\Delta\tau} = -\left(\mathbf{P}_z^0\right)^*\mathbf{h}_x^{n+0.5} + (\mathbf{P}_x^1)^*\frac{\mathbf{h}_z^{n+1} + \mathbf{h}_z^n}{2}, \tag{19b}$$

$$\left(\mathbf{I} + \frac{\Delta\tau^2}{4}\mathbf{P}_y^1(\mathbf{P}_y^1)^* + \frac{\Delta\tau^2}{4}\mathbf{P}_x^1\left(\mathbf{P}_x^1\right)^*\right)\frac{h_z^{n+1} - \mathbf{h}_z^n}{\Delta\tau} = \mathbf{P}_y^1\left(\frac{\mathbf{e}_x^n + \tau}{2}\left[\left(\mathbf{P}_z^1\right)^*\mathbf{h}_y^{n+0.5} - (\mathbf{P}_y^1)^*\mathbf{h}_z^n\right]\right) + \mathbf{P}_x^1\left(-\mathbf{e}_y^n - \frac{\Delta\tau}{2}\left[-\left(\mathbf{P}_z^0\right)^*\mathbf{h}_x^{n+0.5} + (\mathbf{P}_x^1)^*\mathbf{h}_z^n\right]\right). \tag{19c}$$

If the vector $\mathbf{h}_z^{n+1}$ is known, than the first two update equations are explicit ones. The vector $\mathbf{h}_z^{n+1}$ can be found from the third equation, whose solution demands inversion of the matrix

$$\mathbf{W}_{\mathrm{CN}} = \mathbf{I} + \frac{\Delta\tau^2}{4}\mathbf{A} + \frac{\Delta\tau^2}{4}\mathbf{B}, \quad \mathbf{A} = \mathbf{P}_y^1(\mathbf{P}_y^1)^*, \quad \mathbf{B} = \mathbf{P}_x^1(\mathbf{P}_x^1)^*.$$

Eliminating the electric field, Eq. (19c) can be reduced to the form:

$$\mathbf{W}_{\mathrm{CN}}\frac{\mathbf{h}_z^{n+1} - 2\mathbf{h}_z^n + \mathbf{h}_z^{n-1}}{\Delta\tau^2} = -(\mathbf{A} + \mathbf{B})\mathbf{h}_z^n + \mathbf{F}^n, \tag{20}$$

$$\mathbf{F}^n = \mathbf{P}_y^1(\mathbf{P}_z^1)^*\frac{\mathbf{h}_y^{n+0.5} + \mathbf{h}_y^{n-0.5}}{2} + \mathbf{P}_x^1\left(\mathbf{P}_z^0\right)^*\frac{\mathbf{h}_x^{n+0.5} + \mathbf{h}_x^{n-0.5}}{2}. \tag{21}$$

If we assume that vector $\mathbf{F}^n$ is known for all time steps, than Eq. (20) can be identified as the implicit Crank–Nicholson scheme [16] for the two-dimensional wave equation

$$\frac{\partial^2 \mu_z H_z}{\partial \tau^2} = \left(\frac{\partial}{\partial x}\varepsilon_y^{-1}\frac{\partial}{\partial x} + \frac{\partial}{\partial y}\varepsilon_x^{-1}\frac{\partial}{\partial y}\right)H_z + F, \quad \vec{r} \in \Omega \tag{22}$$

with appropriate boundary conditions on boundary $\partial\Omega$.

Of course $\mathbf{F}^n$ is an unknown vector and should be calculated from the already known "TM"-components. However, the stability of the scheme (20) with $\mathbf{F}^n \equiv 0$ is a necessary stability condition to be fulfilled. In the next section we are looking for an economical implicit scheme for the two-dimensional scalar wave equation (22) describing the excitation of *TE*-modes in homogenous waveguides.

4.2. Splitting schemes for two-dimensional scalar wave equation

In order to find an economical scheme three different schemes based on a splitting of the operator $\mathbf{W}_{\mathrm{CN}}$ will be considered.

For the first method we consider the alternating-direction implicit scheme (ADI) [16,26]. Inserting the relation

$$\mathbf{W}_{\mathrm{CN}} = \mathbf{W}_{\mathrm{ADI}} - \mathbf{\Sigma}^n_{\mathrm{ADI}}, \quad \mathbf{W}_{\mathrm{ADI}} = \left(\mathbf{I} + \frac{\Delta\tau^2}{4}\mathbf{A}\right)\left(\mathbf{I} + \frac{\Delta\tau^2}{4}\mathbf{B}\right), \quad \mathbf{\Sigma}_{\mathrm{ADI}} = \frac{\Delta\tau^4}{16}\mathbf{AB}$$

into Eq. (20) leads to the equivalent scheme

$$\mathbf{W}_{\mathrm{ADI}}\frac{\mathbf{h}_z^{n+1} - 2\mathbf{h}_z^n + \mathbf{h}_z^{n-1}}{\Delta\tau^2} = -(\mathbf{A}+\mathbf{B})\mathbf{h}_z^n + \mathbf{F}^n + \tilde{\mathbf{\Sigma}}^n_{\mathrm{ADI}}, \tag{23}$$

$$\tilde{\mathbf{\Sigma}}^n_{\mathrm{ADI}} = \mathbf{\Sigma}_{\mathrm{ADI}}\frac{\mathbf{h}_z^{n+1} - 2\mathbf{h}_z^n + \mathbf{h}_z^{n-1}}{\Delta\tau^2},$$

where the term $\tilde{\mathbf{\Sigma}}^n_{\mathrm{ADI}} = \mathrm{O}(\Delta\tau^4)$ and can be neglected by introducing a splitting error. Note that the splitting error $\tilde{\mathbf{\Sigma}}^n_{\mathrm{ADI}}$ is two orders lower than the approximation error of the scheme.

Scheme (23) without the term $\tilde{\mathbf{\Sigma}}^n_{\mathrm{ADI}} = \mathrm{O}(\Delta\tau^4)$

$$\left(\mathbf{I} + \frac{\Delta\tau^2}{4}\mathbf{A}\right)\left(\mathbf{I} + \frac{\Delta\tau^2}{4}\mathbf{B}\right)\frac{\mathbf{h}_z^{n+1} - 2\mathbf{h}_z^n + \mathbf{h}_z^{n-1}}{\Delta\tau^2} = -(\mathbf{A}+\mathbf{B})\mathbf{h}_z^n + \mathbf{F}^n \tag{24}$$

will be referred as ADI(0) scheme and for the case of diagonal material matrices $\mathbf{M}_{\mu^{-1}}$, $\mathbf{M}_{\varepsilon^{-1}}$ it requires only solving two systems with tri-diagonal matrices.

Unfortunately, scheme (24) is unconditionally stable only for a rectangular domain Ω, when the operators $\mathbf{A}$ and $\mathbf{B}$ are commutative [16]. For an arbitrarily shaped domain Ω the operator $\mathbf{W}_{\mathrm{ADI}}$ is not self-conjugate and the scheme can become unstable even for the time step $\Delta\tau$ equal to the minimal mesh step. To overcome the problem we can retain the term $\tilde{\mathbf{\Sigma}}^n_{\mathrm{ADI}}$ and use an iterative scheme with a small number of iterations. The last method will be called ADI(p), where p represents the number of iterations.

Considering an alternative splitting of the operator

$$\mathbf{W}_{\mathrm{CN}} = \mathbf{W}_{\mathrm{ADI2}} - \mathbf{\Sigma}_{\mathrm{ADI2}}, \ \mathbf{W}_{\mathrm{ADI2}} = \left(\mathbf{I} + \frac{0.5\Delta\tau^2}{4}\mathbf{A}\right)\left(\mathbf{I} + \frac{\Delta\tau^2}{4}\mathbf{B}\right)\left(\mathbf{I} + \frac{0.5\Delta\tau^2}{4}\mathbf{A}\right) - \mathbf{\Sigma}_{\mathrm{ADI2}}, \ \mathbf{\Sigma}_{\mathrm{ADI2}} = \mathrm{O}(\Delta\tau^4),$$

the scheme

$$\mathbf{W}_{\mathrm{ADI2}}\frac{\mathbf{h}_z^{n+1} - 2\mathbf{h}_z^n + \mathbf{h}_z^{n-1}}{\Delta\tau^2} = -(\mathbf{A}+\mathbf{B})\mathbf{h}_z^n + \mathbf{F}^n, \tag{25}$$

with the self-conjugate operator $\mathbf{W}_{\mathrm{ADI2}}$ is obtained. The $\mathbf{\Sigma}^n_{\mathrm{ADI2}}$ term is neglected in the scheme and the latter will be referred to as ADI2. It is also only conditionally stable. But (as verified by numerical experiments) it is stable for larger time steps than the ADI scheme. The second advantage is self-conjugateness of the operator $\mathbf{W}_{\mathrm{ADI2}}$.

In an attempt to find an unconditionally stable economical scheme for wave equation (20), we consider the alternating triangular implicit scheme (ATI) based on the triangular splitting of the operator W_{CN} [16]:

$$\mathbf{W}_{\mathrm{CN}} = \mathbf{I} + \mathbf{L} + \mathbf{L}^* = \mathbf{W}_{\mathrm{ATI}} - \mathbf{\Sigma}_{\mathrm{ATI}}, \quad \mathbf{W}_{\mathrm{ATI}} = (\mathbf{I} + \mathbf{L})(\mathbf{I} + \mathbf{L}^*), \quad \mathbf{\Sigma}_{\mathrm{ATI}} = \mathbf{L}\mathbf{L}^* = \mathrm{O}\left(\frac{\Delta\tau^4}{|\Delta\vec{r}|^2}\right),$$

where $\mathbf{L}$ is a lower triangular matrix. The ATI(0) scheme

$$(\mathbf{I} + \mathbf{L})(\mathbf{I} + \mathbf{L}^*)\frac{\mathbf{h}_z^{n+1} - 2\mathbf{h}_z^n + \mathbf{h}_z^{n-1}}{\Delta\tau^2} = -(\mathbf{A} + \mathbf{B})\mathbf{h}_z^n + \mathbf{F}^n \tag{26}$$

is unconditionally stable. However, it approximates problem (20) only conditionally with error $\mathrm{O}(\Delta\tau^2 + |\Delta\vec{r}|^2 + \frac{\Delta\tau^4}{|\Delta\vec{r}|^2})$ under the approximation condition $\Delta\tau = \mathrm{o}(|\Delta\vec{r}|^{0.5})$. Hence, with the choice $\Delta\tau = \mathrm{O}(|\Delta\vec{r}|)$ the approximation and splitting errors are of the same order. As in the ADI(p) method, the term

$$\tilde{\mathbf{\Sigma}}^n_{\mathrm{ATI}} = \mathbf{\Sigma}_{\mathrm{ATI}}\frac{\mathbf{h}_z^{n+1} - 2\mathbf{h}_z^n + \mathbf{h}_z^{n-1}}{\Delta\tau^2}$$

can be retained and the system can be solved iteratively with p iterations (ATI(p) method).

In order to check stability, accuracy and convergence of the introduced schemes we consider a test problem of free oscillations of the TE mode [27]

$$H_z(\rho, \theta, \tau) = -J_1(k\rho)\cos(\theta)\sin(k\tau), \quad ka = 5.33144, \tag{27}$$

in an infinite perfectly conducting cylinder $\overline{\Omega}$ with radius a:

$$\frac{\partial}{\partial\tau}\varepsilon E_x = \frac{\partial}{\partial y}H_z, \quad \frac{\partial}{\partial\tau}\varepsilon E_y = -\frac{\partial}{\partial x}H_z, \tag{28}$$

$$\frac{\partial}{\partial\tau}\mu H_z = \frac{\partial}{\partial y}E_x - \frac{\partial}{\partial x}E_y, \quad \vec{r} \in \Omega, \quad \tau \in (0, T],$$

$$H_z(\tau = 0) = H_z^0, \quad E_x(\tau = 0) = E_x^0, \quad E_y(\tau = 0) = E_y^0, \quad \vec{r} \in \Omega,$$

$$\vec{n} \times \vec{E} = 0, \quad \vec{r} \in \partial\Omega, \quad \tau \in [0, T],$$

where the initial conditions follow from relation (27).

Problem (28) can be readily reduced to wave equation (22) with the Neumann boundary condition. However, Eq. (22) allows a linearly growing in time solution not available for problem (28). In order to avoid this complication we will solve system (28) directly and for this reason rewrite the schemes introduced above in the form

$$\frac{\mathbf{e}_x^{n+1} - \mathbf{e}_x^n}{\Delta\tau} = -(\mathbf{P}_y^1)^*\frac{\mathbf{h}_z^{n+1} + \mathbf{h}_z^n}{2},$$

$$\frac{\mathbf{e}_y^{n+1} - \mathbf{e}_y^n}{\Delta\tau} = (\mathbf{P}_x^1)^*\frac{\mathbf{h}_z^{n+1} + \mathbf{h}_z^n}{2}, \tag{29}$$

$$\mathbf{W}_* \frac{\mathbf{h}_z^{n+1} - \mathbf{h}_z^n}{\Delta\tau} = \mathbf{P}_y^0 \left(\mathbf{e}_x^n - \frac{\Delta\tau}{2} (\mathbf{P}_y^1)^* \mathbf{h}_z^n \right) + \mathbf{P}_x^0 \left(-\mathbf{e}_y^n - \frac{\Delta\tau}{2} (\mathbf{P}_x^1)^* \mathbf{h}_z^n \right) + \tilde{\mathbf{\Sigma}}_*^n,$$

where the pair $\langle \mathbf{W}_*, \tilde{\mathbf{\Sigma}}_*^n \rangle$ is taken from the set

$$\left\{ \langle \mathbf{W}_{\mathrm{CN}}, \mathbf{0} \rangle, \left\langle \mathbf{W}_{\mathrm{ADI}}, \tilde{\mathbf{\Sigma}}_{\mathrm{ADI}}^n \right\rangle, \langle \mathbf{W}_{\mathrm{ADI2}}, \mathbf{0} \rangle, \left\langle \mathbf{W}_{\mathrm{ATI}}, \tilde{\mathbf{\Sigma}}_{\mathrm{ATI}}^n \right\rangle \right\}$$

and it is assumed that the function $\mathbf{F}^n$ vanishes.

The iterative ADI(p) and ATI(p) schemes take the form

$$\mathbf{W}_* \mathbf{h}_z^{n+1,i} = \widetilde{\mathbf{F}}^n + \tilde{\mathbf{\Sigma}}_*^n \mathbf{h}_z^{n+1,i-1}, \quad i = 1, 2, \ldots, p, \tag{30}$$

where the initial value $\mathbf{h}_z^{n+1,0}$ is obtained from the scheme (29) by neglecting the term $\tilde{\mathbf{\Sigma}}_{\mathrm{ADI}}^n$ or $\tilde{\mathbf{\Sigma}}_{\mathrm{ATI}}^n$, correspondingly.

In the validation example we set the initial field in the entire calculation domain corresponding to the analytically determined eigensolution (27) and start the time-stepping procedures. After a (sufficiently long) period of time $T = 3a/\sqrt{2}$, we compare the numerical solution with the exact one. For simplicity a series of equidistant meshes with the cell sizes $\Delta x = \Delta y = h$ is used.

To achieve a smooth second order convergence for this and for the following numerical examples, a conformal approach for treating perfectly conducting boundaries is chosen. It means that the entries in the permittivity and permeability matrices are changed near the boundary (see [15] and references therein for details).

In the first example the time step is taken as $\Delta\tau = h$. The relative error of the numerical solution $\widetilde{H}_z$

$$\delta(h) = \frac{\left\| H_z - \widetilde{H}_z \right\|_2}{\| H_z \|_2}$$

is shown in Fig. 3. The left figure shows the convergence rates for different non-iterative schemes. The ADI2 scheme (25) achieves the same rate of convergence as the Crank–Nicholson scheme (20). The ADI(0) scheme is unstable. The ATI(0) scheme is stable but it can be seen from the right figure that at least one more iteration (30), than for the ADI2 scheme, is required to achieve the same accuracy.

The Crank–Nicholson scheme conserves the L_2^h norm of the solution [16]. Fig. 4 shows conservation of the discrete energy

$$E_{\mathrm{CN}}^n = 0.5(\langle \mathbf{h}^n, \mathbf{h}^n \rangle + \langle \mathbf{e}^n, \mathbf{e}^n \rangle)$$

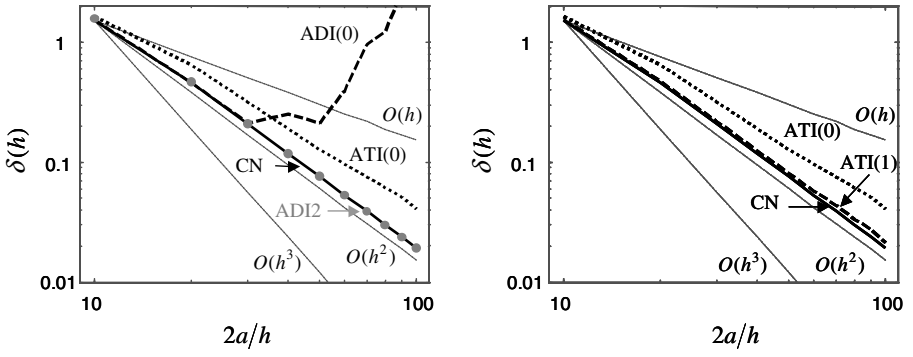

Fig. 3. Comparison of the convergence of different methods for the circle is shown. On the left picture the solid line corresponds to the CN method, the dotted line – to the ATI(0) scheme, dashed line – to the ADI(0) scheme. By gray points the results for the ADI2 method are shown. On the right figure an improvement of the convergence of the ATI(1) scheme (dashed line) compared to the ATI(0) scheme (dotted line) is shown. The solid line describes results from CN method.

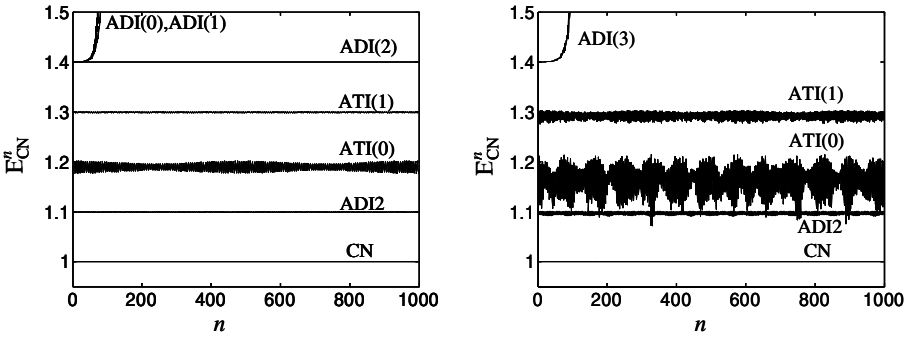

Fig. 4. The discrete energy conservation by different methods is shown. The left figure shows results for the time step $\Delta\tau = h$. The right figure presents the results for the time step $\Delta\tau = 1.5h$.

in the schemes for the mesh resolution $a/h = 10$. The left figure presents the results for the time step $\Delta\tau = h$. The energies are normalized and shifted in order to place them all on the same graph. The schemes ADI(0) and ADI(1) are unstable. The discrete energy in other schemes oscillates near the mean value. The right figure presents likewise the results for the time step $\Delta\tau = 1.5h$. As it can be seen from this figures, the ADI2 scheme shows the best results.

However, as mentioned above the ADI2 scheme is only conditionally stable. It was tested in this example and other geometries that a sufficient stability condition for the conformal ADI2 method can be written in the form

$$\min(\Delta x_i, \Delta y_j) \geqslant 0.5\Delta\tau. \tag{31}$$

In the following we will use the ADI2 splitting in TE/TM scheme (13a), (13b). For the reader interested in elimination of restriction (31) (which indeed is a restriction on a mesh in the transverse plane) we propose to use the TE/TM scheme in conjunction with the unconditionally stable ATI(p) method. However, this possibility will not be studied in this paper. The next section describes only the realization of the ADI2 method in the TE/TM scheme.

4.3. TE/TM-ADI2 scheme in three dimensions

The numerical scheme using the ADI2 splitting in three dimension has the form

$$\mathbf{B}\frac{\mathbf{y}^{n+1}-\mathbf{y}^n}{\Delta\tau} + \mathbf{A}\mathbf{y}^n = \mathbf{f}^n, \tag{32}$$

where

$$\mathbf{B} = \begin{pmatrix} \mathbf{I} - 0.5\Delta\tau\mathbf{D}_{11} + \mathbf{\Sigma}^1_{\mathrm{ADI2}} & \mathbf{0} \\ \Delta\tau\mathbf{D}^*_{12} & \mathbf{I} - 0.5\Delta\tau\mathbf{D}_{22} + \mathbf{\Sigma}^2_{\mathrm{ADI2}} \end{pmatrix}, \mathbf{A} = \begin{pmatrix} -\mathbf{D}_{11} & -\mathbf{D}_{12} \\ \mathbf{D}^*_{12} & -\mathbf{D}_{22} \end{pmatrix},$$

$$\mathbf{y}^n = \begin{pmatrix} \mathbf{u}^{n-0.5} \\ \mathbf{v}^n \end{pmatrix}, \quad \mathbf{f}^n = \begin{pmatrix} \mathbf{j}^n_u \\ \mathbf{j}^{n+0.5}_v \end{pmatrix}.$$

As for the TE/TM scheme (13) the relations

$$\mathbf{A} = -\mathbf{A}^*, \quad \mathbf{Q} = \mathbf{Q}^*, \quad \mathbf{Q} = \mathbf{B} - 0.5\Delta\tau\mathbf{A},$$

and Theorem 2 hold. However, the stable time step does now not only depend on the longitudinal mesh step Δz but also on the minimal mesh step in the transverse plane. Hence, the stability conditions (16) and (31) have to be combined in the common empiric inequality

$$\Delta\tau \leqslant \min(2\Delta x_i, 2\Delta y_j, \Delta z). \tag{33}$$

The last condition does not reduce the applicability of the scheme, since the field is relatively smooth in the transverse plane and a much coarser grid can be used here. As it was already mentioned, constraint (33) can be relaxed and replaced by (16) if the ATI(p) method is used.

So far we have not defined the ADI2 terms in relation (32). Instead of doing this, let us rewrite scheme (32) explicitly

$$\frac{\widehat{\mathbf{h}}_x^{n+0.5} - \widehat{\mathbf{h}}_x^{n-0.5}}{\Delta\tau} = \mathbf{M}_{\mu_x^{-1}}\left[\mathbf{P}_z\widehat{\mathbf{e}}_y^{n} - \mathbf{P}_y\frac{\widehat{\mathbf{e}}_z^{n+0.5} + \widehat{\mathbf{e}}_z^{n-0.5}}{2}\right], \tag{34a}$$

$$\frac{\widehat{\mathbf{h}}_y^{n+0.5} - \widehat{\mathbf{h}}_y^{n-0.5}}{\Delta\tau} = -\mathbf{M}_{\mu_y^{-1}}\left[\mathbf{P}_z\widehat{\mathbf{e}}_x^{n} - \mathbf{P}_x\frac{\widehat{\mathbf{e}}_z^{n+0.5} + \widehat{\mathbf{e}}_z^{n-0.5}}{2}\right], \tag{34b}$$

$$\begin{aligned}\mathbf{W}^e_{\mathrm{ADI2}}\frac{\widehat{\mathbf{e}}_z^{n+0.5} + \widehat{\mathbf{e}}_z^{n-0.5}}{2} &= \mathbf{M}_{\varepsilon_z^{-1}}\mathbf{P}_y^*\left(\widehat{\mathbf{h}}_x^{n-0.5} + \frac{\Delta\tau}{2}\mathbf{M}_{\mu_x^{-1}}\left[\mathbf{P}_z\widehat{\mathbf{e}}_y^{n} - \mathbf{P}_y\widehat{\mathbf{e}}_y^{n-0.5}\right]\right)\\ &+ \mathbf{M}_{\varepsilon_z^{-1}}\mathbf{P}_x^*\left(-\widehat{\mathbf{h}}_y^{n-0.5} - \frac{\Delta\tau}{2}\mathbf{M}_{\mu_y^{-1}}\left[-\mathbf{P}_z\widehat{\mathbf{e}}_x^{n} + \mathbf{P}_x\widehat{\mathbf{e}}_y^{n-0.5}\right]\right) + \mathbf{M}_{\varepsilon_z^{-1}}\widehat{\mathbf{j}}_y^{n-0.5},\end{aligned} \tag{34c}$$

$$\frac{\widehat{\mathbf{e}}_x^{n+1} - \widehat{\mathbf{e}}_x^{n}}{\Delta\tau} = \mathbf{M}_{\varepsilon_x^{-1}}\left[\mathbf{P}_z^*\widehat{\mathbf{h}}_y^{n+0.5} - \mathbf{P}_y^*\frac{\widehat{\mathbf{h}}_z^{n+1} + \widehat{\mathbf{h}}_z^{n}}{2}\right], \tag{35a}$$

$$\frac{\widehat{\mathbf{e}}_y^{n+1} - \widehat{\mathbf{e}}_y^{n}}{\Delta\tau} = -\mathbf{M}_{\varepsilon_y^{-1}}\left[\mathbf{P}_z^*\widehat{\mathbf{h}}_x^{n+0.5} - \mathbf{P}_x^*\frac{\widehat{\mathbf{h}}_z^{n+1} + \widehat{\mathbf{h}}_z^{n}}{2}\right], \tag{35b}$$

$$\begin{aligned}\mathbf{W}^h_{\mathrm{ADI2}}\frac{\mathbf{h}_z^{n+1} - \mathbf{h}_z^{n}}{\Delta\tau} &= \mathbf{M}_{\mu_z^{-1}}\mathbf{P}_y\left(\widehat{\mathbf{e}}_x^{n} + \frac{\Delta\tau}{2}\mathbf{M}_{\varepsilon_x^{-1}}\left[\mathbf{P}_z^*\widehat{\mathbf{h}}_y^{n+0.5} - \mathbf{P}_y^*\widehat{\mathbf{h}}_z^{n}\right]\right)\\ &+ \mathbf{M}_{\mu_z^{-1}}\mathbf{P}_x\left(-\widehat{\mathbf{e}}_y^{n} - \frac{\Delta\tau}{2}\mathbf{M}_{\varepsilon_y^{-1}}\left[-\mathbf{P}_z^*\widehat{\mathbf{h}}_x^{n+0.5} + \mathbf{P}_x^*\widehat{\mathbf{h}}_z^{n}\right]\right),\end{aligned} \tag{35c}$$

where

$$\mathbf{W}^h_{\mathrm{ADI2}} = \left(\mathbf{I} + \frac{\Delta\tau^2}{8}\mathbf{M}_{\mu_z^{-1}}\mathbf{P}_y\mathbf{M}_{\varepsilon_x^{-1}}\mathbf{P}_y^*\right)\left(\mathbf{I} + \frac{\Delta\tau^2}{4}\mathbf{M}_{\mu_z^{-1}}\mathbf{P}_x\mathbf{M}_{\varepsilon_y^{-1}}\mathbf{P}_x^*\right)\left(\mathbf{I} + \frac{\Delta\tau^2}{8}\mathbf{M}_{\mu_z^{-1}}\mathbf{P}_y\mathbf{M}_{\varepsilon_x^{-1}}\mathbf{P}_y^*\right),$$

$$\mathbf{W}^e_{\mathrm{ADI2}} = \left(\mathbf{I} + \frac{\Delta\tau^2}{8}\mathbf{M}_{\varepsilon_z^{-1}}\mathbf{P}_y^*\mathbf{M}_{\mu_x^{-1}}\mathbf{P}_y\right)\left(\mathbf{I} + \frac{\Delta\tau^2}{4}\mathbf{M}_{\varepsilon_z^{-1}}\mathbf{P}_x^*\mathbf{M}_{\mu_y^{-1}}\mathbf{P}_x\right)\left(\mathbf{I} + \frac{\Delta\tau^2}{8}\mathbf{M}_{\varepsilon_z^{-1}}\mathbf{P}_y^*bfM_{\mu_x^{-1}}\mathbf{P}_y\right).$$

If material matrices $\mathbf{M}_{\mu^{-1}}, \mathbf{M}_{\varepsilon^{-1}}$ are diagonal, then systems (34c), (35c) have only products of tri-diagonal matrices on the left-hand side and can be easily resolved. For example, Eq. (34c) leads to the set of equations

$$
\begin{aligned}
&(\mathbf{I}+0.5\mathbf{A})\mathbf{u}_1=\mathbf{F}^n,\quad (\mathbf{I}+\mathbf{B})\mathbf{u}_2=\mathbf{u}_1,\\
&(\mathbf{I}+0.5\mathbf{A})\widehat{\mathbf{e}}_x^{\,n+0.5}=(\mathbf{I}+0.5\mathbf{A})\widehat{\mathbf{e}}_x^{\,n-0.5}+\mathbf{u}_2,
\end{aligned}
\tag{36}
$$

where the vector $\mathbf{F}^n$ denotes the right-hand side of Eq. (34c) and

$$
\mathbf{A}=\frac{\Delta\tau^2}{4}\mathbf{M}_{\varepsilon_z^{-1}}\mathbf{P}_y^*\mathbf{M}_{\mu_x^{-1}}\mathbf{P}_y,\quad \mathbf{B}=\frac{\Delta\tau^2}{4}\mathbf{M}_{\varepsilon_z^{-1}}\mathbf{P}_x^*\mathbf{M}_{\mu_y^{-1}}\mathbf{P}_x. \tag{37}
$$

However, the conformal scheme with the diagonal material matrices reduces the stable time step. To restore stability condition (33) and the possibility to use the time step $\Delta\tau=\Delta z$, we will use a modification of the uniformly stable conformal method [25] as described in detail in [15]. The last approach results in modified non-diagonal but symmetric matrices $\mathbf{M}_{\mu_x^{-1}}$, $\mathbf{M}_{\varepsilon_y^{-1}}$. Other material matrices in scheme (34), (35) remain diagonal. This means that we do not encounter difficulties in the resolution of Eq. (35c). However, resolving Eq. (34c) requires additional efforts since the matrices (37) are not tri-diagonal.

To overcome the problem we modify system (36) as follows:

$$
\begin{aligned}
&(\mathbf{I}+0.5\mathbf{A}_0)\mathbf{u}_1=\mathbf{F}^n-(\mathbf{A}_1+\mathbf{B}_1)(\widehat{\mathbf{e}}_z^{\,n+0.5}-\widehat{\mathbf{e}}_z^{\,n-0.5}),\\
&(\mathbf{I}+\mathbf{B}_0)\mathbf{u}_2=\mathbf{u}_1,\quad (\mathbf{I}+0.5\mathbf{A}_0)\widehat{\mathbf{e}}_z^{\,n+0.5}=(\mathbf{I}+0.5\mathbf{A}_0)\widehat{\mathbf{e}}_z^{\,n-0.5}+\mathbf{u}_2,
\end{aligned}
\tag{38}
$$

where

$$
\mathbf{A}_0=\frac{\Delta\tau^2}{4}\mathbf{M}_{\varepsilon_z^{-1}}\mathbf{P}_y^*\mathbf{M}^0_{\mu_x^{-1}}\mathbf{P}_y,\quad \mathbf{B}_0=\frac{\Delta\tau^2}{4}\mathbf{M}_{\varepsilon_z^{-1}}\mathbf{P}_x^*\mathbf{M}^0_{\mu_y^{-1}}\mathbf{P}_x,\quad \mathbf{A}_1=\mathbf{A}-\mathbf{A}_0,\quad \mathbf{B}_1=\mathbf{B}-\mathbf{B}_0,
$$

and $\mathbf{M}^0_{\mu_x^{-1}},\mathbf{M}^0_{\varepsilon_y^{-1}}$ are diagonal parts of the material matrices. System (38) can be resolved iteratively

$$
\begin{aligned}
&\mathbf{G}^i=\begin{cases}0, & i=0,\\ (\mathbf{A}_1+\mathbf{B}_1)(\widehat{\mathbf{e}}_z^{\,n+0.5,i-1}-\widehat{\mathbf{e}}_z^{\,n-0.5}), & i>0,\end{cases}\\
&(\mathbf{I}+0.5\mathbf{A}_0)\mathbf{u}_1^i=\mathbf{F}^n+\mathbf{G}^i,\quad (\mathbf{I}+\mathbf{B}_0)\mathbf{u}_2^i=\mathbf{u}_1^i,\\
&(\mathbf{I}+0.5\mathbf{A}_0)\widehat{\mathbf{e}}_z^{\,n+0.5,i}=(\mathbf{I}+0.5\mathbf{A}_0)\widehat{\mathbf{e}}_z^{\,n-0.5}+\mathbf{u}_2^i,\quad i=0,1,2,\ldots,p.
\end{aligned}
\tag{39}
$$

Note that the equation for zero iteration (which we refer to as TE/TM-ADI2(0)), just as schemes (36) and (38), results in an approximation of the continuous problem (1) with the error $O(|\Delta\vec{r}|^2+\Delta\tau^2)$. However, the TE/TM-ADI2(0) scheme can show instability in general geometries for the required time step $\Delta\tau=\Delta z$. The first iteration (which we refer as TE/TM-ADI2(1) scheme) solves the stability problem for all considered cases.

In the next section, we will study properties of the scheme (32)–(39) for the case of rotationally symmetric geometries. In the last section results for the fully three-dimensional scheme will be presented.

5. Verification of the TE/TM scheme

5.1. Realization of TE/TM and TE/TM-ADI2 schemes for rotationally symmetric geometries

In this section we describe the realization of the TE/TM scheme for the case of rotationally symmetric geometries. We consider this case separately since the TE/TM scheme (13a), (13b) is already economical and application of the splitting methods considered in the previous sections can be avoided.

For a bunch moving at speed of light c at an offset a from and parallel to the axis of a rotationally symmetric structure, the source current $\vec{j}$ can be represented as

$$\vec{j} = \frac{\vec{c}\rho(z/c - t)\delta(r - a)}{\pi a} \sum_{m=0}^{\infty} \frac{\cos m\varphi}{1 + \delta_{m0}},$$

where $\rho(s)$ is the longitudinal charge distribution and m is the azimuthal mode number.

Numerical scheme (13) for an azimuthal mode number m has the form

$$\begin{aligned}
&\frac{\widehat{\mathbf{h}}_{\varphi}^{n+0.5} - \widehat{\mathbf{h}}_{\varphi}^{n-0.5}}{\Delta\tau} = \mathbf{M}_{\mu_{\varphi}^{-1}} \left[\mathbf{P}_z \widehat{\mathbf{e}}_r^{n} - \mathbf{P}_r \frac{\widehat{\mathbf{e}}_z^{n+0.5} + \widehat{\mathbf{e}}_z^{n-0.5}}{2} \right],\\
&\frac{\widehat{\mathbf{h}}_{r}^{n+0.5} - \widehat{\mathbf{h}}_{r}^{n-0.5}}{\Delta\tau} = -\mathbf{M}_{\mu_{r}^{-1}} \left[\mathbf{P}_z \widehat{\mathbf{e}}_{\varphi}^{n} - m \frac{\widehat{\mathbf{e}}_z^{n+0.5} + \widehat{\mathbf{e}}_z^{n-0.5}}{2} \right],\\
&\mathbf{W}_{\mathrm{CN}}^{e} \frac{\widehat{\mathbf{e}}_z^{n+0.5} - \widehat{\mathbf{e}}_z^{n-0.5}}{\Delta\tau} = \mathbf{M}_{\varepsilon_z^{-1}} \mathbf{P}_r^{*} \left(\frac{\widehat{\mathbf{h}}_{\varphi}^{n-0.5} + \tau}{2} \mathbf{M}_{\mu_{\varphi}^{-1}} \left[\mathbf{P}_z \widehat{\mathbf{e}}_r^{n} - \mathbf{P}_r \widehat{\mathbf{e}}_z^{n-0.5} \right] \right)\\
&\qquad + \mathbf{M}_{\varepsilon_z^{-1}} \mathbf{P}_{\varphi}^{*} \left(- \frac{\widehat{\mathbf{h}}_{r}^{n-0.5} - \tau}{2} \mathbf{M}_{\mu_{r}^{-1}} \left[-\mathbf{P}_z \widehat{\mathbf{e}}_{\varphi}^{n} + m \widehat{\mathbf{e}}_z^{n-0.5} \right] \right) + \mathbf{M}_{\varepsilon_z^{-1}} \widehat{\mathbf{j}}_z^{n},\\
&\frac{\widehat{\mathbf{e}}_{\varphi}^{n+1} - \widehat{\mathbf{e}}_{\varphi^n}}{\Delta\tau} = \mathbf{M}_{\varepsilon_{\varphi}^{-1}} \left[\mathbf{P}_z^{*} \widehat{\mathbf{h}}_r^{n+0.5} - \mathbf{P}_r^{*} \frac{\widehat{\mathbf{h}}_z^{n+1} + \widehat{\mathbf{h}}_z^{n}}{2} \right],\\
&\frac{\widehat{\mathbf{e}}_{r}^{n+1} - \widehat{\mathbf{e}}_{r}^{n}}{\Delta\tau} = -\mathbf{M}_{\varepsilon_{r}^{-1}} \left[\mathbf{P}_z^{*} \widehat{\mathbf{h}}_{\varphi}^{n+0.5} - m \frac{\widehat{\mathbf{h}}_z^{n+1} + \widehat{\mathbf{h}}_z^{n}}{2} \right],\\
&\mathbf{W}_{\mathrm{CN}}^{h} \frac{\mathbf{h}_z^{n+1} - \mathbf{h}_z^{n}}{\Delta\tau} = \mathbf{M}_{\mu_z^{-1}} \mathbf{P}_r \left(\widehat{\mathbf{e}}_{\varphi}^{n} + \frac{\Delta\tau}{2} \mathbf{M}_{\varepsilon_{\varphi}^{-1}} \left[\mathbf{P}_z^{*} \widehat{\mathbf{h}}_r^{n+0.5} - \mathbf{P}_r^{*} \widehat{\mathbf{h}}_z^{n} \right] \right)\\
&\qquad + \mathbf{M}_{\mu_z^{-1}} \mathbf{P}_{\varphi} \left(-\widehat{\mathbf{e}}_r^{n} - \frac{\Delta\tau}{2} \mathbf{M}_{\varepsilon_r^{-1}} \left[-\mathbf{P}_z^{*} \widehat{\mathbf{h}}_{\varphi}^{n+0.5} + m \widehat{\mathbf{h}}_z^{n} \right] \right),
\end{aligned} \tag{40}$$

$$\begin{aligned}
&\mathbf{W}_{\mathrm{CN}}^{h} = \left(\mathbf{I} + \frac{\Delta\tau^2}{4} \mathbf{M}_{\mu_z^{-1}} \mathbf{P}_r \mathbf{M}_{\varepsilon_{\varphi}^{-1}} \mathbf{P}_r^{*} + \frac{\Delta\tau^2}{4} m^2 \mathbf{M}_{\mu_z^{-1}} \mathbf{M}_{\varepsilon_r^{-1}} \right),\\
&\mathbf{W}_{\mathrm{CN}}^{e} = \left(\mathbf{I} + \frac{\Delta\tau^2}{4} \mathbf{M}_{\varepsilon_z^{-1}} \mathbf{P}_r^{*} \mathbf{M}_{\mu_{\varphi}^{-1}} \mathbf{P}_r + \frac{\Delta\tau^2}{4} m^2 \mathbf{M}_{\varepsilon_z^{-1}} \mathbf{M}_{\mu_r^{-1}} \right),
\end{aligned} \tag{41}$$

and the fact that $\mathbf{P}_{\varphi} = m\mathbf{I}$ is used.

If the material matrices $\mathbf{M}_{\mu^{-1}}$, $\mathbf{M}_{\varepsilon^{-1}}$ are diagonal, then operators (41) are tri-diagonal matrices and equations involving them can be resolved easily. For the case of non-diagonal matrices $\mathbf{M}_{\mu_{\varphi}^{-1}}$, $\mathbf{M}_{\mu_r^{-1}}$ we will proceed in the same way as described at the end of the previous section.

We rewrite the equation with the operator $\mathbf{W}_{\mathrm{CN}}^{e}$ in the form

$$(\mathbf{I} + \mathbf{A}_0 + \mathbf{B}_0) \left(\widehat{\mathbf{e}}_z^{n+0.5} - \widehat{\mathbf{e}}_z^{n-0.5} \right) = \mathbf{F}^{n} - (\mathbf{A}_1 + \mathbf{B}_1)(\widehat{\mathbf{e}}_z^{n+0.5} - \widehat{\mathbf{e}}_z^{n-0.5}), \tag{42}$$

where

$$\mathbf{A}_0 = \frac{\Delta\tau^2}{4} \mathbf{M}_{\varepsilon_z^{-1}} \mathbf{P}_r^{*} \mathbf{M}_{\mu_{\varphi}^{-1}}^{0} \mathbf{P}_r, \quad \mathbf{B}_0 = \frac{\Delta\tau^2}{4} m^2 \mathbf{M}_{\varepsilon_z^{-1}} \mathbf{M}_{\mu_r^{-1}}^{0}, \quad \mathbf{A}_1 = \mathbf{A} - \mathbf{A}_0, \quad \mathbf{B}_1 = \mathbf{B} - \mathbf{B}_0,$$

and $\mathbf{M}_{\mu_{\varphi}^{-1}}^{0}$, $\mathbf{M}_{\mu_r^{-1}}^{0}$ are diagonal parts of the material matrices. System (42) can be resolved iteratively

$$\mathbf{G}^i = \begin{cases} 0, & i = 0, \\ (\mathbf{A}_1 + \mathbf{B}_1)(\widehat{\mathbf{e}}_z^{\,n+0.5,i-1} - \widehat{\mathbf{e}}_z^{\,n-0.5}), & i > 0, \end{cases} \tag{43}$$

$$(\mathbf{I} + \mathbf{A}_0 + \mathbf{B}_0)\widehat{\mathbf{e}}_z^{\,n+0.5,i} = (\mathbf{I} + \mathbf{A}_0 + \mathbf{B}_0)\widehat{\mathbf{e}}_z^{\,n+0.5} + \mathbf{F}^n + \mathbf{G}^i, \quad i = 0, 1, 2, \ldots, p.$$

Scheme (40)–(43) will be referred to as TE/TM(p). Note that just as for the TE/TM-ADI2(p) scheme, it is sufficient to perform only one iteration (scheme TE/TM(1)) to obtain a stable solution.

As it was noted at the beginning of this section, for geometries of revolution we do not need to apply the transverse operator splitting. However, to check the achieved accuracy the TE/TM-ADI2(p) scheme was implemented for rotationally symmetric geometries, too.

As test example we consider free oscillations of the TM mode [27]

$$H_\varphi(r,\theta,\varphi,\tau) = k\frac{(kr)^{0.5}}{r}J_{1.5}(kr)\frac{\partial}{\partial\theta}P_1^1(\cos(\theta))\cos(\varphi)\sin(k\tau), \quad H_r(r,\theta,\varphi,\tau) = 0,$$

$$H_\theta(r,\theta,\varphi,\tau) = k\frac{(kr)^{0.5}}{r\sin(\theta)}J_{1.5}(kr)P_1^1(\cos(\theta))\sin(\varphi)\sin(k\tau), \quad ka = 6.116764,$$

in the sphere of radius $a = 1$.

The initial field is converted to the cylindrical coordinates and set in the entire calculation domain. After a period of time $T = \sqrt{2}a$ we compare the numerical solution with the exact one. A series of equidistant meshes with the cell sizes $r = z = h$ is used.

Fig. 5 shows the results for the time step $\Delta\tau = \Delta z$ and for the mesh resolution $a/h = 10$. The left figure shows convergence of the non-iterative schemes TE/TM(0) (40)–(43) and TE/TM-ADI2(0) (32)–(39). Both schemes achieve the same rate of convergence. The right figure shows conservation of the discrete energy $E^n_{\mathrm{TE/TM}}$ for the schemes. With an increase of the number of iterations p the discrete energy in the TE/TM(p) scheme converges to the constant value of the non-iterative TE/TM scheme. However, in order to see the same effect for the TE/TM-ADI2(p) scheme, the energy norm has to be changed to the one with operator $\mathbf{Q}$ from the non-iterative scheme (32). We do not show this result here, since it already follows from the available figure that the considered schemes are stable for time step $\Delta\tau = \Delta z$, when they do not have dispersion in the longitudinal direction.

As a further test example we use the circular collimator structure shown in Fig. 6 on the left (with inner radius b not indicated in the figure). Fig. 7 shows the results for the dipole wake field ($m = 1$) and compares the TE/TM scheme results to the ones obtained with the classical Yee's scheme (E/M scheme). The latter results are calculated with the help of code ABCI [28] (FDTD method with triangular approximation of the boundary). The geometric parameters are $a = 35$ mm, $L = 20$ cm and $b = c = 2$ mm, where b is an inner radius of the collimator.

The left figure in Fig. 7 shows the transversal dipole wake potential [1]

$$W_\perp^1(s) = \left|\mathbf{W}_\perp^1(s,r,\theta=0)\right| r^{-1}, \quad \mathbf{W}_\perp^1(s,r,\theta) = \frac{1}{Q}\int_{-\infty}^{\infty}\left[\mathbf{E}_\perp + (v\times\mathbf{B})_\perp\right]_{t=(z+s)/v}\mathrm{d}z$$

for the collimator with $L = 20$ cm and the relativistic Gaussian bunch with RMS length $\sigma = 1$ mm. The solid curves show the results for ABCI and the dashed ones present the results for the new scheme.

In the right figure the transversal dipole loss factor

$$L_\perp^1 = \frac{1}{Q}\int_{-\infty}^{\infty} W_\perp^1(s)\rho(s)\,\mathrm{d}s$$

for the collimator is shown for different mesh resolutions σ/h, where $h = z = r$ is the mesh step. The error compared to the reference value (obtained with the finest mesh resolution) is also shown in the figure. The dashed line shows the results for the TE/TM code and the solid line for ABCI.

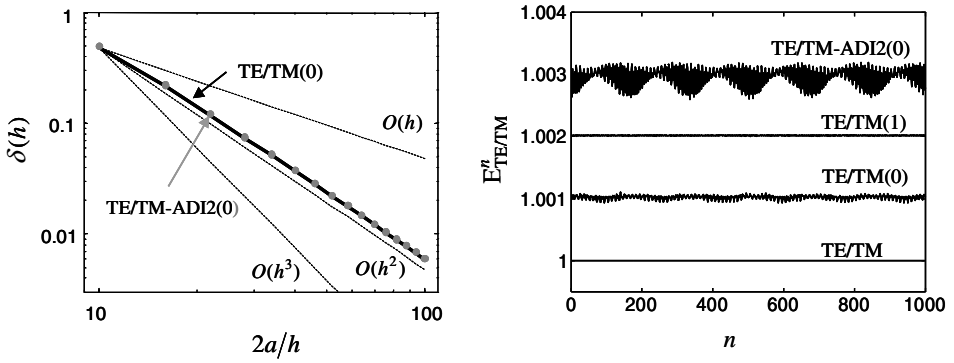

Fig. 5. The left figure shows second order convergence of the TE/TM(0) (solid line) and TE/TM-ADI2(0) schemes for the sphere. The right figure presents conservation of the discrete energy by different methods for $\Delta\tau = \Delta z$.

From the above example we see that the absolute error for the new TE/TM scheme just as for scheme [14,15] remains approximately on the same level independently from the length of the collimator. The reference code ABCI demands a much more dense mesh for the same accuracy, strongly depending on the collimator length.

Finally, we show in Fig. 8 (left) the dipole wake potentials of a Gaussian bunch with $\sigma = 1$ mm for the TESLA cryomodule of total length ~11 m [29]. The cryomodule contains eight cavities and nine bellows whose geometries are outlined in Fig. 9. The iris' radius is 35 mm and the beam tube's radius is 39 mm.

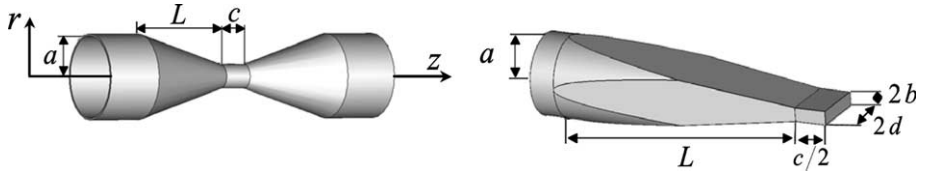

Fig. 6. The geometry of round and rectangular collimators.

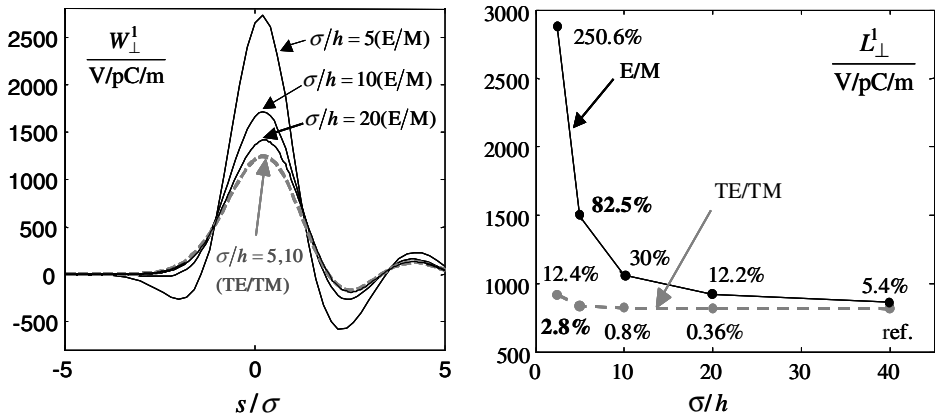

Fig. 7. The transverse dipole wake function (left) and loss factor (right) for the collimator with $L = 20$ cm. The solid lines show the results for the E/M scheme (Yee's scheme) and the dashed lines display the results for the TE/TM scheme. The relative errors are given regarding the reference value (marked as ref. on the graphs) calculated by the TE/TM method with the finest mesh.

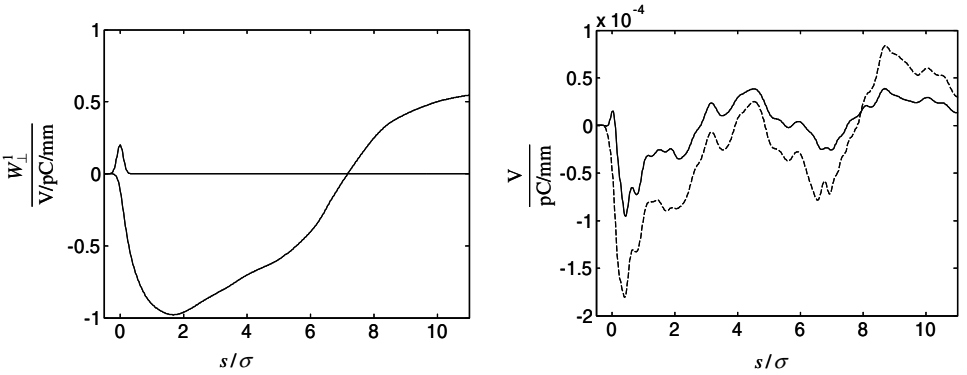

Fig. 8. The left figure shows the transverse wake potential for the TESLA cryomodule excited by the Gaussian bunch with RMS width $\sigma = 1$ mm as obtained from the reference code [15]. On the right figure the solid line shows the difference between the reference potential and the one obtained with the help of the TE/TM(1) scheme and the dashed line shows likewise the result for the TE/TM-ADI2(1) scheme.

The moving mesh in the last example covers the bunch longitudinally in the range from -5σ to 100σ. The length of the moving mesh is only 0.105 m which results in a drastically reduction of the computational demands (storage and CPU time) compared to the stationary mesh of total length $\sim$11 m.

The right figure shows the difference between the results obtained by the TE/TM(1) and TE/TM-ADI2(1) schemes and the reference result calculated with the vector potential method (POT-2.5) described in [14,15]. The presented results are calculated with the mesh resolution $\Delta z = \Delta r = \sigma/5$. It can be seen that the new methods introduced in this paper produce numerical results of the same level of accuracy as the vector potential method (POT-2.5). However, the TE/TM method is at least two times faster due to the smaller number of required operations.

5.2. Numerical examples calculated with the three-dimensional TE/TM-ADI2 scheme

Finally, we discuss the results of numerical computations with the fully three-dimensional realization of the TE/TM-ADI2(p) scheme (32)–(39). Two test problems are considered.

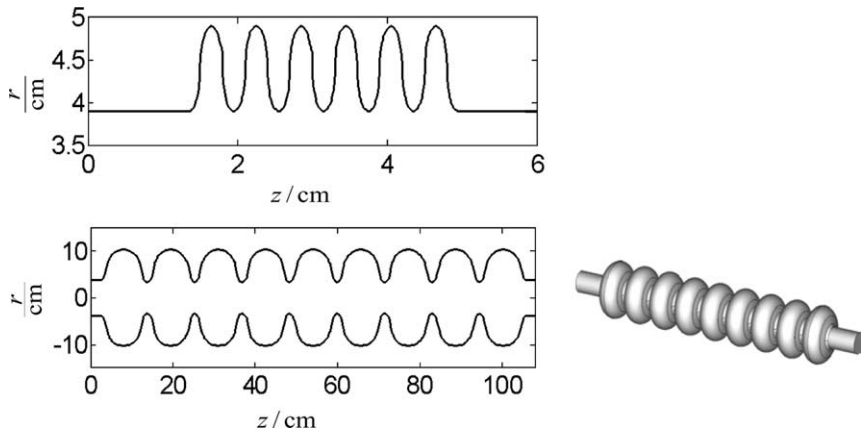

Fig. 9. The geometry of the TESLA cavity (bottom) and bellow (top).

Before presentation of the numerical results we want to discuss shortly the realization of the scheme in the code. To be able to calculate long structures, we should spare the computer memory and not keep all geometric information. For this purpose we cut the long structure in short blocks, discritize them and keep the geometric information in the external memory. The information will be loaded only at the instant when the head of the bunch arrives at a geometric block and it will be deleted after bunch (together with the moving mesh) have passed through the block.

To be able to check the accuracy of the three-dimensional realization of the TE/TM scheme we have chosen only rotationally symmetric structures for the numerical tests. However, in the three-dimensional calculations the symmetry of the structures was not exploited.

In the first example we consider a structure consisting of the 20 TESLA cells [29] bounded by infinite ingoing and outgoing pipes with diameter 35 mm. Analytical solution (3) was used as an initial condition in the ingoing pipe.

Fig. 10 shows the longitudinal wake potential [1]

$$W_{\parallel}(s,x,y) = -\frac{1}{Q}\int_{-\infty}^{\infty}[E_z(x,y,z,t)]_{t=(z+s)/v}\,\mathrm{d}z$$

for a Gaussian bunch with RMS length $\sigma = 1$ mm moving on the axis. The solid line (POT-2.5D) corresponds to the reference solution obtained with the vector potential method [15]. The two other lines show results obtained with different mesh resolutions from the TBCI code [6] based on the classical Yee's scheme (E/M-2.5D). The oscillations, that appear, are due to the dispersion error of the Yee's scheme. The gray points present the result obtained by the three-dimensional scheme (32)–(39) (marked as TE/TM-3D).

It can be seen that the three-dimensional TE/TM-ADI2 scheme produces very accurate results even for the coarse mesh. Indeed, the three-dimensional code uses only 2.5 mesh points per σ in the longitudinal direction. In the transverse direction the mesh steps are even three times bigger.

As the next example we use again the round collimator. Fig. 11 demonstrates the wake potential for the collimator with parameters $a = 30$ mm, $b = 2$ mm, $c = 50$ mm, $L = 200$ mm and a Gaussian bunch with RMS length $\sigma = 1$ mm. Again the high accuracy of the suggested three-dimensional scheme can be seen.

Finally, in the last example we calculate the longitudinal wake potential for the fully three-dimensional rectangular collimator shown in Fig. 6 on the right. Fig. 12 demonstrates the wake potential for the

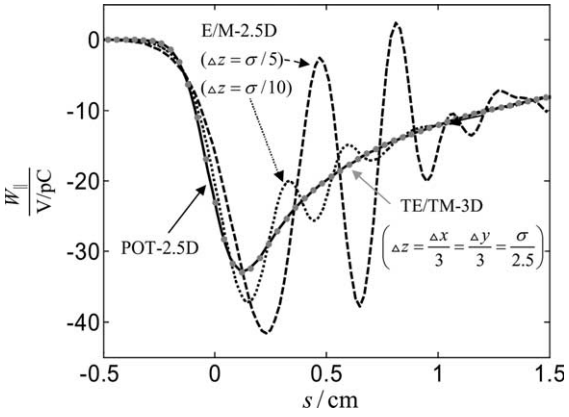

Fig. 10. Comparison of the wake potentials obtained by different methods for the structure consisting of 20 TESLA cells excited by a Gaussian bunch with $\sigma = 1$ mm. The solid line shows the reference solution obtained with the help of the scheme described in [15]. The dashed line describes the solution obtained by classical Yee's scheme with mesh resolution of five mesh steps per σ. The dotted line describes the solution obtained by Yee's scheme with two times denser resolution in the longitudinal direction. The picture shows coincidence of the reference result (solid line) with the results on the coarse mesh obtained from the 3D TE/TM code (gray points).

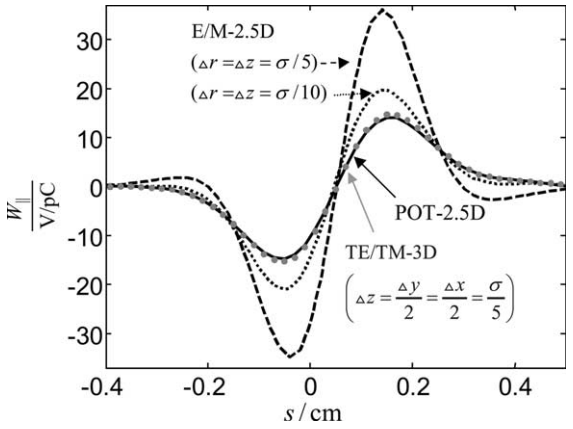

Fig. 11. Comparison of the wake potentials obtained by different methods for the round collimator excited by a Gaussian bunch with $\sigma = 1$ mm. The solid line shows the reference solution obtained with the help of the scheme described in [15]. The dashed line shows the solution obtained by Yee's scheme with a mesh resolution of five mesh steps on σ. The dotted line describes the solution obtained by Yee's scheme with two times denser resolution. The picture shows coincidence of the reference result (solid line) with the results on the coarse mesh obtained from the 3D TE/TM code (gray points).

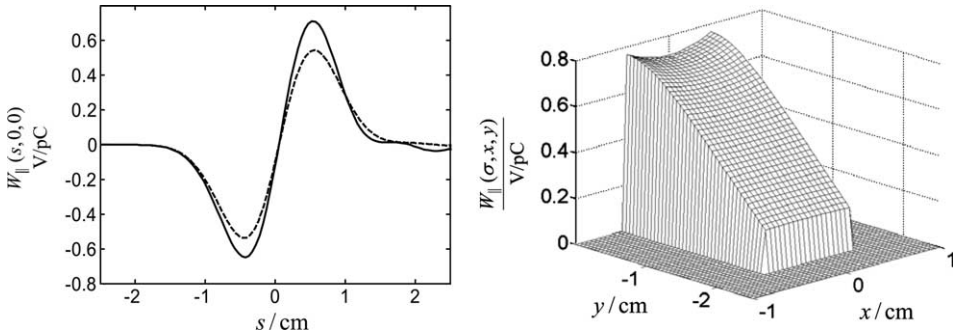

Fig. 12. The left figure shows the longitudinal wake potential on the axis for rectangular (solid line) and circular (dashed lines) collimators and a Gaussian bunch with $\sigma = 5$ mm. On the right picture the energy gain for a test particle moving at the position $s = \sigma$ behind the bunch centre is shown.

collimator with parameters $a = 30$ mm, $b = 5$ mm, $d = 20$ mm, $c = 50$ mm, $L = 200$ mm and a Gaussian bunch with RMS length $\sigma = 5$ mm moving on the axis. Fig. 12 (left) compares the wake potential on the axis for the rectangular (solid line) and round (dashed line) collimators. The round collimator has the same geometric parameters and the round aperture with radius $b = 5$ mm. As well known, the wake potential of a round collimator does not change in the transverse plane. Quite contrary, for the rectangular collimator a variation of the wake potential in the transverse plane is expected. Indeed, it can be seen in Fig. 12 (right), where the energy gain for a test particle moving at the position $s = \sigma$ behind the bunch centre is shown.

6. Conclusion

A new fully three-dimensional implicit scheme for the calculation of electromagnetic fields in the vicinity of relativistic charged bunches was introduced. As shown by several numerical examples, the scheme is able to model curved boundaries with high accuracy and allows for a non-deteriorating calculation of the field solution for very long simulation times.

To develop the new scheme we proceeded as follows: first we replaced the E/M splitting of Yee's scheme by the TE/TM splitting. This resulted in an implicit scheme requiring the solution of the Crank–Nicholson equation for the two-dimensional scalar wave equation. In order to find an accurate economical scheme, three different splitting methods were considered. It was shown that the ADI2 approach results in an accurate scheme with moderate restriction on the time step. We then introduced the TE/TM scheme based on the ADI2 method and studied several test examples. In order to avoid reduction of the maximal time step and to obtain a scheme without dispersion in the longitudinal direction the conformal approach with non-diagonal material matrices was exploited. It requires the application of iterative procedures. However, already the first iteration produces an accurate and stable solution for all considered examples.

The high overall accuracy of the scheme was demonstrated for realistic collimator problems. The scheme allows to use a moving mesh and thus to calculate wake fields of very short bunches for a range of problems, for which presently available 3D codes experience severe problems.

Acknowledgement

The authors thank R. Schuhmann for helpful discussions.

References

[1] B.W. Zotter, S.A. Kheifets, Impedances and Wakes in High-energy Particle Accelerators, World Scientific, London, 1998.
[2] V. Balakin, A. Novokhatskii, et al., Beam dynamics of colliding electron-positron beams, in: Proceedings of the 6th All-Union Conference on Charged-Particle Accelerators, USSR, 1978.
[3] T. Weiland, Transient electromagnetic fields excited by bunches of charged particles in cavities of arbitrary shape, in: Proceedings of the 11th International Conference on High-Energy Accelerators, Geneva, Switzerland, 1980.
[4] K.S. Yee, Numerical solution of initial boundary value problems involving Maxwell's equations in isotropic media, IEEE Trans. Antennas Propag. 14 (1966) 302.
[5] MAFIA Collaboration, MAFIA manual, CST GmbH, Darmstadt, 1997.
[6] T. Weiland, TBCI and URMEL – New computer codes for wake field and cavity mode calculations, IEEE Trans. Nucl. Sci. 30 (1983) 2489.
[7] S. Wang, F.L. Teixeira, Dispersion-relation-preserving FDTD algorithms for large-scale three-dimensional problems, IEEE Trans. Antennas Propag. 51 (2003) 1818.
[8] N.V. Kantartzis, T.T. Zygiridis, T.D. Tsiboukis, An unconditionally stable higher order ADI-FDTD technique for the dispersionless analysis of generalized 3-D EMC structures, IEEE Trans. Magn. 40 (2004) 1436.
[9] J.B. Cole, High-accuracy Yee algorithm based on nonstandard finite differences: new developments and verifications, IEEE Trans. Antennas Propag. 50 (2002) 1185.
[10] T. Kashiwa, et al., Phase velocity errors of the nonstandard FDTD method and comparison with other high-accuracy FDTD methods, IEEE Trans. Magn. 39 (2003) 2125.
[11] R. Hampel, I. Zagorodnov, T. Weiland, New discretization scheme for wake field computation in cylindrically symmetric structures, in: Proceedings of the EPAC 2004, Lucerne, p. 2556.
[12] A. Mosnier, A. Novokhatskii, Wakefield dynamics in quasi-periodic structures, in: Proceedings of the PAC 1997, Vancouver, Canada.
[13] A. Novokhatski, M. Timm, T. Weiland, Transition dynamics of the wake fields of ultra short bunches, TESLA Report 2000-03, DESY, 2000.
[14] I. Zagorodnov, T. Weiland, Calculation of transversal wake potential for short bunches, in: Proceedings of the ICAP 2002, East Lansing.
[15] I. Zagorodnov, R. Schumann, T. Weiland, Long-time computation of electromagnetic fields in the vicinity of a relativistic source, J. Comput. Phys. 191 (2003) 525.
[16] A.A. Samarskii, The Theory of Difference Schemes, Marcel Dekker, New York, 2001.
[17] A.A. Samarskii, P.P. Matus, P.N. Vabischevich, Difference Schemes with Operator Factors, Kluwer Academic Publishers, London, 2002.
[18] T. Namiki, 3D ADI- FDTD method – Unconditionally stable time-domain algorithm for solving full vector Maxwell's equations, IEEE Trans. Microwave Theory Tech. 48 (2000) 1743.

[19] J. Lee, B. Fornberg, Some unconditionally stable time stepping methods for the 3-D Maxwell's equations, J. Comput. Appl. Math. 166 (2004) 497.
[20] W.C. Chao, Physics of Collective Beam Instabilities in High Energy Accelerators, Wiley, New York, 1993.
[21] T. Weiland, Time domain electromagnetic field computation with finite difference methods, Int. J. Numer. Model. 9 (1996) 295.
[22] T. Weiland, On the unique numerical solution of Maxwellian eigenvalue problems in three dimensions, Particle Accelerators 17 (1985) 227.
[23] R. Schuhmann, T. Weiland, Conservation of discrete energy and related laws in the finite integration technique, in: PIER Manograph Series 32, 2001, p. 301.
[24] F. Edelvik, R. Schuhmann, T. Weiland, A general stability analysis of FIT/FDTD applied to lossy dielectrics and lumped elements, Int. J. Numer. Model. 17 (2004) 407.
[25] I. Zagorodnov, R. Schuhmann, T. Weiland, A uniformly stable conformal FDTD-method on Cartesian grids, Int. J. Numer. Model. 16 (2003) 127.
[26] J. Douglas Jr., S. Kim, H. Lim, An improved alternating-direction method for a viscous wave equation, Contemp. Math. 329 (2003) 99.
[27] K. Simonyi, Foundations of Electrical Engineering, Pergamon Press, Oxford, 1963.
[28] Y.H. Chin, User's guide for ABCI Version 8.7, CERN-SL-94-02-AP, CERN, 1994.
[29] TESLA Technical Design Report, DESY 2001-011, Hamburg, Germany, 2001, Part II.